Applied Catalysis B: Environmental 84 (2008) 482–489

Contents lists available at ScienceDirect

Applied Catalysis B: Environmental

journal homepage: www.elsevier.com/locate/apcatb

Hydrodesulfurization of thiophene on carbon nanofiber supported Co/Ni/Mo catalysts

Zhixin Yu [a], Lars Erik Fareid [a], Kjell Moljord [a,b], Edd A. Blekkan [a], John C. Walmsley [c,d], De Chen [a,*]

[a] Department of Chemical Engineering, Norwegian University of Science and Technology (NTNU), N-7491 Trondheim, Norway
[b] Statoil Research Center, Postuttak, N-7005 Trondheim, Norway
[c] SINTEF Materials and Chemistry, N-7491 Trondheim, Norway
[d] Department of Physics, Norwegian University of Science and Technology (NTNU), N-7491 Trondheim, Norway

ARTICLE INFO

Article history:
Received 9 January 2008
Received in revised form 25 April 2008
Accepted 10 May 2008
Available online 24 May 2008

Keywords:
Carbon nanofiber
Co/Ni/Mo
Hydrodesulfurization
Thiophene

ABSTRACT

Co, Mo, NiMo and CoMo catalysts supported on alumina, fishbone and platelet carbon nanofibers (CNFs) have been prepared. The dispersion of the oxide phases was qualitatively studied and compared using X-ray diffraction (XRD) and transmission electron microscopy (TEM). The reducibility of the catalysts was studied by temperature programmed reduction (TPR). Hydrodesulfurization (HDS) of thiophene was used as a model reaction to compare the activity of different catalysts. The activity tests showed that the alumina supported catalysts exhibited higher activity compared to the corresponding CNF supported catalysts, and the NiMo catalysts were more active than the corresponding CoMo catalysts. The thiophene HDS activity was correlated with the dispersion of the molybdenum species and the reducibility of different catalysts. Interestingly, the CNF supported Co catalysts have higher thiophene HDS activity than the CNF supported Co(Ni)Mo catalysts.

1. Introduction

Hydrodesulfurization (HDS) is an important process which has received much attention in recent years due to environmental and clean-fuel legislation. In this process compounds containing sulfur undergo reaction with hydrogen and form the corresponding hydrocarbon and hydrogen sulfide. Industrial HDS processes are usually carried out on supported sulfided CoMo or NiMo catalysts. Alumina is the most widely used support material for commercial HDS catalysts due to its good mechanical and textural properties [1,2]. Other notable features of alumina supports include their ability to provide high dispersion of the active metal components. However, it has also been shown that chemical interactions exist between the alumina and transition metal oxides in the precursor state. Some of the species formed are very stable and resistant to complete sulfidation [3,4].

Carbon has been shown to be promising as catalyst support for HDS, because carbon supported molybdenum based catalysts have shown superior HDS activity compared with the alumina supported counterparts [4–7]. The much higher activity has been ascribed to an enhanced dispersion of the metal species due to the large surface area of the carbon supports, and to a weak metal-support interaction, which is beneficial for the complete sulfidation of catalytic precursors.

However, carbon supported catalysts have not been extensively utilized in industrial HDS processes due to the extremely high microporosity of carbon, which typically have a pore size largely below 2 nm and will exert serious diffusion limitations on bulky reactants or cause pore plugging by coke [4]. In this respect, nanostructured carbon like carbon nanofibers (CNFs) and carbon nanotubes (CNTs) appear to be interesting candidates because they are almost exclusively mesoporous. In addition to the mesoporosity, the CNFs and CNTs are characterized by high purities, high mechanical strengths, high thermal stability and tunable bulk density [8–10].

Dong et al. [11] and Shang et al. [12,13] have reported that multi-walled carbon nanotubes supported CoMo catalysts had higher activity for thiophene or dibenzothiophene HDS than activated carbon or γ-Al_2O_3 supported catalysts. The high activity of CoMo/CNT was explained by the number of anion vacancies in the active phases, in spite of that the active phase is not well dispersed on the support. The other reason for the high activity of the CoMo/CNT was suggested to be a combination of the electron donor effect of the CNTs and the so-called nanosize effect [12].

Previous studies have reported that different carbon nanostructures have significant impact on the activity and selectivity of the supported catalysts, in for example hydrogenation of crotonaldehyde [14], oxidative dehydrogenation of ethylbenzene

* Corresponding author. Tel.: +47 73 59 31 49; fax: +47 73 59 50 47.
E-mail address: chen@nt.ntnu.no (D. Chen).

0926-3373/$ – see front matter © 2008 Elsevier B.V. All rights reserved.
doi:10.1016/j.apcatb.2008.05.013

[15] and Fischer–Tropsch synthesis [16]. It has been shown that the CNFs are superior to CNTs for these reactions in terms of catalyst activity and selectivity due to the large number of edge sites presented on the surface, which are the anchoring sites for the active metal species. To the best of our knowledge, no studies on the CNFs supported molybdenum HDS catalysts have been reported. Therefore, the present work aims at exploring CNFs supported molybdenum based HDS catalysts and elucidating the effect of graphite sheet orientation of different carbon nanostructures on the structure and HDS activity of different catalysts. A comparison between the CNF supports and a γ-Al_2O_3 support is also included. In addition, no detailed kinetic study of the catalyst activity and deactivation have been reported for carbon nanostructures supported HDS catalysts, hence the other purpose in this work is to study the kinetic behavior of the CNFs supported catalysts in thiophene HDS.

In the literature, studies on HDS over both CoMo and NiMo catalysts have been reported. CoMo was found to be a better catalyst for lighter fractions, while NiMo was more active towards heavier fractions or deep HDS, and was much less sensitive to amines than the Mo and CoMo catalysts [17,18]. For comparison, both CoMo and NiMo were chosen in the present work, and the CNFs supported molybdenum and cobalt-only catalysts have also been tested in thiophene HDS.

2. Experimental

2.1. Catalyst preparation

Platelet CNFs, fishbone CNFs and commercial γ-Al_2O_3 have been used as supports. The platelet CNFs have their graphite sheets perpendicular to the fiber axis, while the fishbone CNFs have the graphite sheets oriented at an angle to the fiber axis. The pore volumes of platelet, fishbone and γ-Al_2O_3 supports are 0.33, 0.25 and 0.50 cm^3/g, respectively. The BET surface areas are 172, 88 and 193 m^2/g, respectively.

The platelet CNFs used in this study were prepared from CO decomposition on a Fe_3O_4 catalyst [19], while the fishbone CNFs were prepared from CO decomposition on a 20 wt.% Ni/SiO_2 catalyst [20]. After growth, the CNFs were boiled in concentrated nitric acid solution (65%) for 3 h in order to introduce surface oxygen groups and remove catalyst particles. The fishbone CNFs were also refluxed in 3 M NaOH solution to remove SiO_2. After the treatments the CNFs were washed with large amounts of water and dried in air at 373 K overnight.

A series of Mo, CoMo and NiMo catalysts were prepared using the standard incipient wetness method. The molybdenum-only catalysts were prepared by one-step incipient wetness with an aqueous solution containing the desired amount of $(NH_4)_6Mo_7O_{24}{\cdot}4H_2O$ (99%, Merck). The solution was heated carefully to ensure that $(NH_4)_6Mo_7O_{24}$ was completely dissolved before impregnation. For the bimetallic catalysts, a two-step incipient wetness method was used: $(NH_4)_6Mo_7O_{24}{\cdot}4H_2O$ was first applied to the support, then the sample was dried at 110 °C for 3 h, and then $Co(NO_3)_2{\cdot}6H_2O$ (99%, Fluka) or $Ni(NO_3)_2{\cdot}6H_2O$ (99%, Merck) was added and the sample was dried at 110 °C overnight. The molar ratio of Co(Ni)/Mo is 1:3 which has been demonstrated as the optimal ratio for the HDS catalysts [11,21]. All the Mo containing catalysts were calcined in flowing N_2 at 350 °C for 5 h with a ramp rate of 2 °C/min. One CoMo catalyst supported on platelet has been calcined in N_2 at 500 °C for 5 h.

The cobalt-only catalysts were prepared by wet impregnation with toluene/ethanol (2:1, v/v) solutions of $Co(NO_3)_2{\cdot}6H_2O$ [22]. For this preparation, the required amount of $Co(NO_3)_2{\cdot}6H_2O$ dissolved in 100 ml toluene/ethanol was added to 10 g of CNFs. The catalysts were dried at 120 °C overnight, and calcined in flowing N_2 at 300 °C. These cobalt-only catalysts have previously been employed and studied extensively for Fischer–Tropsch synthesis in our group. As the change of calcination temperature from 300 to 350 °C will not have any influence on the structure of the catalysts, the two Co/CNF catalysts were used for thiophene HDS without re-calcination at 350 °C. Hydrogen chemisorption study showed that the Co/Platelet has a high dispersion of 12.2%, while the Co/Fishbone catalyst has a moderate dispersion of 6.7%.

Table 1
Metal loadings of different catalysts, their corresponding denotations and the thiophene conversion on these catalysts

Metal loading (wt.%)			Support	Denotation	Conversion[a] (%)
Mo	Co	Ni			
	12		Fishbone	Co/Fishbone	19.2
	12		Platelet	Co/Platelet	23.0
12			Fishbone	Mo/Fishbone	3.8
12			Al_2O_3	Mo/Al_2O_3	5.5
12	4		Fishbone	CoMo/Fishbone	12.7
12	4		Platelet	CoMo/Platelet	11.9
12	4		Al_2O_3	CoMo/Al_2O_3	14.6
12		4	Fishbone	NiMo/Fishbone	17.8
12		4	Platelet	NiMo/Platelet	18.1
12		4	Al_2O_3	NiMo/Al_2O_3	26.5

[a] Thiophene conversion at 381 min (after the system and the catalyst were stabilized).

The metal loadings on different supports and the denotations for the resulting catalysts are summarized in Table 1.

2.2. Catalyst characterization

X-ray diffraction (XRD) patterns were recorded for calcined catalysts at room temperature by a Siemens D5005 X-ray diffractometer using Cu Kα radiation (λ = 1.54 Å). The scans were recorded in the 2θ range between 20° and 75° using a step size of 0.03°. Peaks were identified by comparison with standards in a database.

For temperature programmed reduction (TPR) experiments, approximately 0.2 g of a calcined catalyst was exposed to a reducing gas mixture consisting of 7% H_2 in argon, while the temperature was increased at 10 °C/min from ambient temperature to 930 °C. A cold trap containing a mixture of 2-propanol and dry ice was used to eliminate water and other condensable products from the product gas mixtures. The consumption of hydrogen was measured by analyzing the effluent gas with a thermal conductivity detector.

Transmission electron microscopy (TEM) study was performed with a JEOL 2010F electron microscope. TEM specimens were prepared by ultrasonic dispersion of the catalyst samples in ethanol, and then a drop of the suspension was applied to a holey carbon support grid. The TEM characterization has been performed for both calcined and sulfided catalysts. The instrument was also operated in the scanning transmission electron microscope (STEM) mode and Energy dispersive X-ray analysis (EDX) mapping was performed for one calcined NiMo/Fishbone catalyst.

2.3. Hydrodesulfurization of thiophene

For HDS experiments, gaseous thiophene was added to the H_2 gas stream by bubbling it through liquid thiophene in a glass saturator kept at 0 °C. The reactions were carried out in a stainless steel tubular microreactor with a steel mesh supporting the catalysts [18]. The temperature was monitored by a thermocouple positioned in a metal tube in the reactor directly below the catalyst bed.

For each reaction, 0.1 g catalyst was diluted with SiC (88 μm) in a weight ratio of 1:10 to avoid hot spots in the catalyst bed. Above the catalyst bed, coarse SiC particles (~5 g) were placed to obtain an evenly distributed temperature profile in the reaction mixture flow upstream of the catalyst bed.

The sulfiding of the catalysts was carried out by passing 60 ml/min H_2S/H_2 (5% vol H_2S) mixture through the reactor. The reactor was heated from room temperature to the sulfiding temperature (407 °C) at a heating rate of 10 °C/min and kept at 407 °C for 1 h. The reactor was then cooled down to the reaction temperature (300 °C) under H_2S/H_2 flow, and the reaction was started by passing the H_2/thiophene mixture (molar ratio 37) through the reactor. The vapor pressure of thiophene at these conditions was 2484.9 Pa [18] and the total flow was 100 ml/min for all experiments. The reaction pressure was always maintained 0.1 MPa. The products were analyzed online using an Agilent 6890 N gas chromatograph equipped with a HP-5 5% Phenyl Methyl Siloxane capillary column (300 m × 320 μm × 0.25 μm).

3. Results and discussion

3.1. XRD characterization

Fig. 1 shows the XRD patterns of the calcined Mo/Al_2O_3 and Mo/Fishbone catalysts, and the diffraction patterns of CoMo/Fishbone and Co/Fishbone are included for comparison. For the Mo/Al_2O_3 catalyst, there are no peaks attributable to any crystalline molybdenum compounds, but only broad peaks of the alumina support (Fig. 1(a)). This implied that a homogeneous distribution of the precursors or no crystalline molybdenum oxide is formed on the surface of alumina. This is in agreement with the results of Chen et al. [12], who found that for the alumina supported CoMo catalysts, the active phase strongly interacts with the –OH groups of alumina which results in a high dispersion. Indeed, Mo/Al_2O_3 catalysts are often referred to as monolayer systems, due to the tendency of the active phase to spread over the support at elevated temperature. In this way, an overlayer of MoO_x is formed on the support surface, and the surface free energy of the system is minimized. Thermodynamics dictate that bulk MoO_x is only formed when the alumina surface is completely covered [23].

In contrast, the Mo/Fishbone catalyst presents diffraction peaks of MoO_3, with the characteristic peaks located at around 23.2°, 25.8° and 27.3°, as shown in Fig. 1(b). The active phases seem to be not as well dispersed on the fishbone CNFs, since it displays apparent reflections of MoO_3. The possible reason is that the aqueous molybdenum salt solution does not easily wet the surface of the CNFs during impregnation. The main diffraction at $2\theta = 26°$ is characteristic of the (0 0 2) diffraction plane of graphite. The peak is somewhat broadened, implying that the degree of long-range order of CNFs was relatively low compared with that of graphite [11].

If cobalt is added to the catalysts, the $CoMo/Al_2O_3$ catalyst still only displays reflections of the alumina support, but no any observable MoO_x or $CoMoO_x$ diffractions (not shown). The diffraction pattern of the CoMo/Fishbone catalyst is very similar to the diffractions of Mo/Fishbone: displaying characteristic peaks of graphite and MoO_3 (Fig. 1(c)). There are no apparent reflections of separate cobalt oxide species. However, it is very possible that bimetallic CoMo oxides are formed, because the diffraction of the mixed oxide $CoMoO_4$ is mostly overlapping with that of MoO_3, with characteristic 2θ angles located at 23.2°, 26.5° and 27.3°. The most obvious difference between the diffractions of CoMo/Fishbone and Mo/Fishbone is that the former has lower intensity, implying a smaller particle size and thus better dispersion of the molybdenum species. Therefore, the addition of cobalt seems to increase the dispersion of molybdenum, probably because CNF supports are more favorable for evenly distributed Co and Ni than Mo [24], and the resulting mixed CoMo oxide will have a higher dispersion compared with Mo oxide. As expected, the diffraction pattern of Co/Fishbone presents peaks attributable to CNFs and Co_3O_4, as shown in Fig. 1(d).

The diffraction pattern of the CoMo/Platelet catalyst is identical with that of CoMo/Fishbone (Fig. 2(a) vs. Fig. 1(c)). Therefore, different carbon nanostructures do not result in different Co or Mo phases in the calcined catalysts. However, the intensity of the molybdenum oxides on platelet CNFs is very low, lower than the peak intensity on fishbone CNFs. This indicates small catalyst particles on the platelet CNFs and a better dispersion of Mo species on platelet than on fishbone. This might be a result of a higher surface area and pore volume of the platelet CNFs or the larger number of edge sites presented on platelet CNFs [16,25]. The characteristic CNF peaks are also slightly different, which can be explained by their different nanostructures and crystallinity.

Fig. 2 also shows the diffraction pattern of the CoMo/Platelet catalyst calcined in N_2 at 500 °C. Apart from the peaks of CNFs, peaks are observed at 2θ of 26.1°, 37.0°, 54.5°, 60.5° and 66.9°. The peaks are ascribed to the MoO_2 phase, not the expected MoO_3. In addition, there are weak diffraction peaks at 23.2° and 27.3°, which

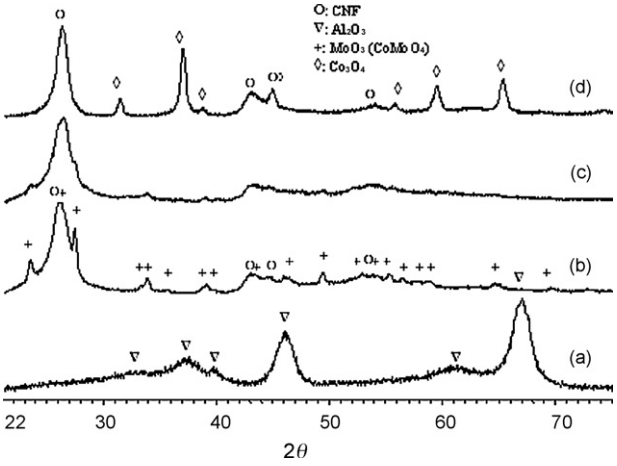

Fig. 1. XRD patterns of the supported Co/Mo/CoMo catalysts; (a) Mo/Al_2O_3, (b) Mo/Fishbone, (c) CoMo/Fishbone, and (d) Co/Fishbone. For clarity the peaks of CoMo/Fishbone are not marked.

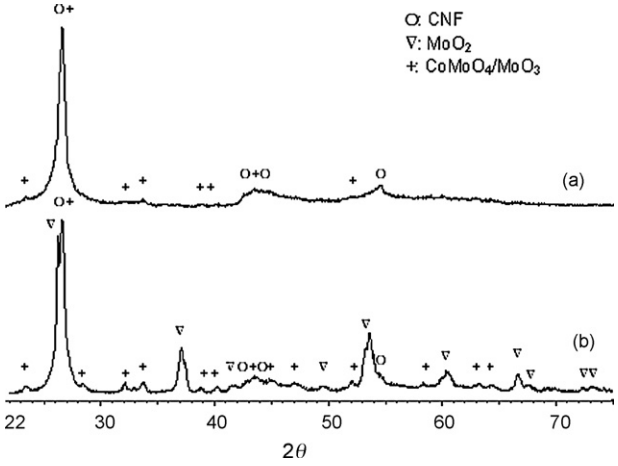

Fig. 2. XRD patterns of the CoMo/Platelet catalysts calcined at different temperatures; (a) CoMo/Platelet calcined at 350 °C, and (b) CoMo/Platelet calcined at 500 °C.

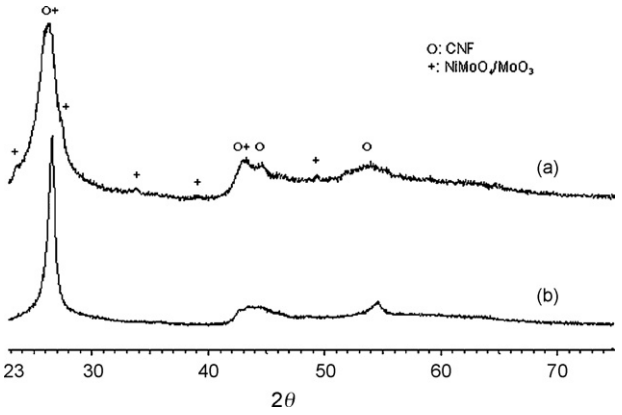

Fig. 3. XRD patterns of the supported NiMo catalysts; (a) NiMo/Fishbone, and (b) NiMo/Platelet.

are due to either $CoMoO_4$ or MoO_3. Therefore, there is another phase ascribed to MoO_2 formed on the platelet CNF. It appears that MoO_3 was partly reduced into the low valence state MoO_2 by CNFs when the calcination temperature was increased from 350 to 500 °C. This is in accordance with previous observations, and can be explained by the reduction ability of the carbon materials [26,27].

The CoMo/Platelet catalyst calcined at 500 °C also displays peaks with higher intensity, indicating that the active phase conglomerates into larger crystallites after high temperature treatment. The interaction between the active phases and the CNFs is relatively weak, and mobilization and conglomeration of the active phases may occur during the heat treatment process.

Fig. 3 shows the diffraction patterns of the NiMo/Fishbone and NiMo/Platelet catalysts, which are very similar to the reflections of Mo/Fishbone and CoMo/Fishbone. The identified diffraction peaks correspond to CNFs, MoO_3 and/or $NiMoO_4$. Nickel also seems to form bimetallic phases with Mo instead of forming separate nickel oxide species. The lower intensity of the MoO_3/$NiMoO_4$ peaks again suggests that the dispersion is higher compared with the molybdenum-only catalysts (Fig. 1(b)), and the particle sizes are small. The NiMo/Platelet catalyst also has smaller diffraction peaks than NiMo/Fishbone, due to the higher surface area of the platelet CNFs.

3.2. Temperature programmed reduction

TPR characterization gives a good indication of the degree of interaction of Ni(Co)Mo with the supports. Fig. 4 shows the TPR profiles of the CoMo catalysts on different supports. The reduction of CoMo catalysts supported on CNFs occurs in the temperature range of 300–750 °C. The CoMo/Platelet catalyst only has one

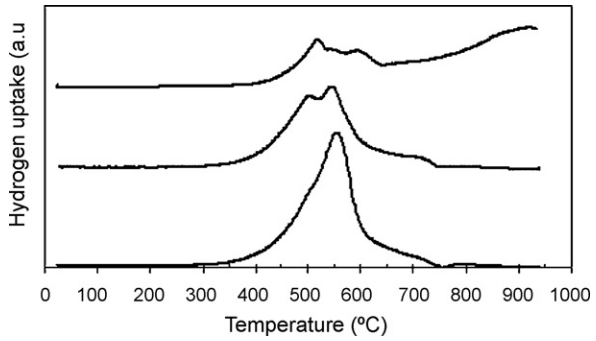

Fig. 4. TPR profiles of the supported CoMo catalysts. From top: CoMo/Alumina, CoMo/Fishbone, CoMo/Platelet.

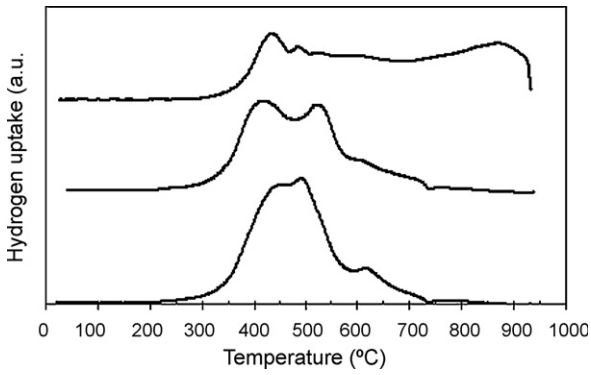

Fig. 5. TPR profiles of the supported NiMo catalysts. From top: NiMo/Alumina, NiMo/Fishbone, NiMo/Platelet.

hydrogen uptake peak at 555 °C, although a very small shoulder at around 500 °C is present before it reaches the peak maximum. The CoMo/Fishbone catalyst has two reduction peaks at 505 and 545 °C. The fishbone CNF supported catalyst is slightly easier to reduce than the platelet supported one. Because of the complexity of the bimetallic system, it is difficult to assign the hydrogen consumption peaks to the reduction of specific Co or Mo oxide phases.

In contrast, $CoMo/Al_2O_3$ has three main hydrogen consumption peaks at 520, 595, and >900 °C. The reduction is not complete even at 930 °C, due to the reduction of highly dispersed molybdenum oxide species strongly interacting with the alumina support. The high temperature reduction peak has been frequently observed for γ-alumina supported catalyst systems and has been ascribed to the strong interaction between the small precursor species and the alumina support [28,29]. Clearly, alumina presents a much stronger interaction compared with the fishbone and platelet CNFs.

Both the NiMo/Platelet and NiMo/Fishbone materials complete their reduction at around 730 °C (Fig. 5). For NiMo/Platelet, the hydrogen consumption peaks are located at 450 and 495 °C. For NiMo/Fishbone, the two major reduction peaks are located at 420 and 525 °C. The reduction peaks of both catalysts are relatively broad. The reduction of NiMo/Platelet is slightly easier than that of NiMo/Fishbone. The $NiMo/Al_2O_3$ catalyst has main reduction peaks at 435, 530 and 870 °C. Similar as the $CoMo/Al_2O_3$ catalyst (Fig. 4), the last peak is attributed to the reduction of molybdenum oxide species that interact strongly with alumina.

It is apparent that the NiMo catalysts are reduced at a lower temperature than the CoMo catalysts (Figs. 4 and 5). This can be explained by the higher reducibility of Ni compared with Co. The reduction of Ni or Co will promote the reduction of molybdenum oxides by hydrogen spillover, because hydrogen can be dissociated on the more easily reduced Ni or Co sites at comparatively lower temperatures; such hydrogen spills to the molybdenum oxide sites and reduces them [30,31].

It has been reported previously that there is a good correspondence of the reducibility of the molybdenum catalysts and their HDS activity [27]. This is because the sulfiding process of a catalyst is combined with the reduction of the oxides by hydrogen. The whole process is usually done in excess of both reducing and sulfiding agent and a catalyst that is easily reduced also easily undergoes sulfidation at the same conditions, resulting in a higher percentage of active species and higher activity of the catalysts.

3.3. Transmission electron microscopy

TEM characterization has been performed on the CNFs supported catalysts to obtain an overview of the particle size

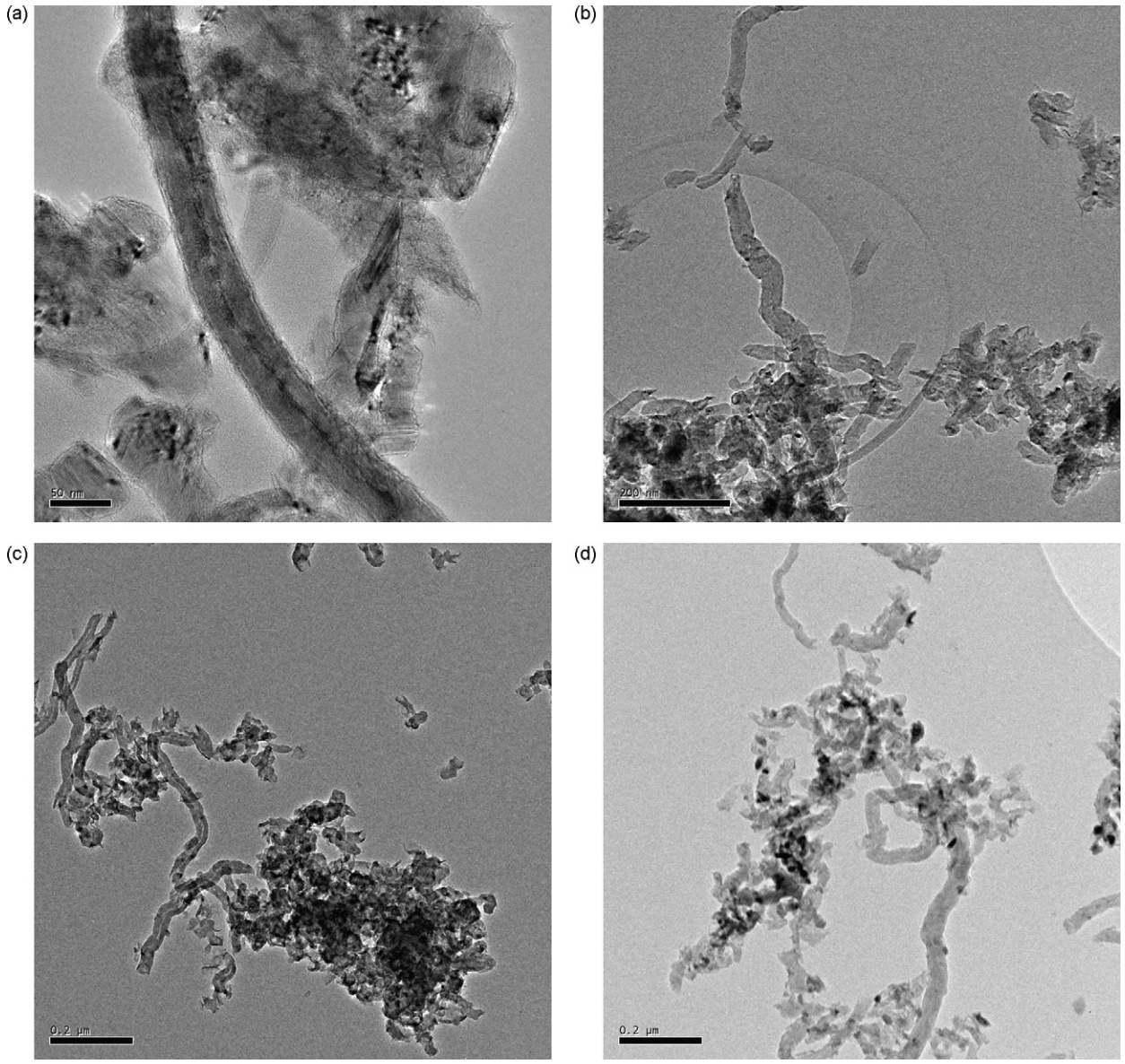

Fig. 6. TEM images of (a) CoMo/Platelet, (b) CoMo/Fishbone, (c) NiMo/Fishbone, and (d) sulfided CoMo/Fishbone.

and dispersion of the bimetallic catalysts. Fig. 6(a) is a representative image of the CoMo/Platelet catalyst after calcination in nitrogen. The fibers seem to be cut to shorter lengths to some extent after boiling in concentrated nitric acid for 3 h. Instead of forming a monolayer on the CNFs, CoMo and/or Mo oxide particles are observed on the surface of the fibers. The particles are small in size and are more or less homogeneous, in agreement with the low intensity of the diffraction peaks observed from the XRD study.

For the CoMo/Fishbone catalyst, an overview image is shown as Fig. 6(b). Similar as the platelet CNFs, the fishbone CNFs were cut into shorter lengths after boiling in nitric acid. CoMo and/or Mo oxide particles are also deposited as small particles on the CNF surface, and these small particles have contributed to the small diffraction peaks observed in the XRD diffractogram. The observation from TEM on the NiMo/Fishbone catalyst is similar to that on CoMo/Fishbone: metal oxide precursors are deposited as small particles on the surface, but not coating the CNF surfaces. Occasionally, some conglomerates consisting of a large number of small NiMo oxide particles can be seen, which could be formed during calcination (Fig. 6(c)).

The CoMo/Fishbone catalyst after sulfidation has also been subjected to TEM study for comparison, as displayed in Fig. 6(d). Compared with the CoMo/Fishbone after calcination, the CoMo and/or Mo sulfide particles are apparently larger. This can be explained by species mobility during the reduction and sulfiding process.

As molybdenum oxide very easily forms a monolayer on alumina, which is not the case found on the CNFs supports, STEM-EDX was performed on the calcined NiMo/Fishbone catalyst to further confirm that. The instrument was operated in the dark field mode and an overview of the studied catalyst is shown as Fig. 7(a), where the scanned area is marked by the pink rectangle. Fig. 7(b) is the sum spectrum from the EDX analysis. It clearly shows that the main components of the catalyst are Ni and Mo (Be and Cu are from the TEM sample holder and sample support). There are no impurities such as Si, which might come from the catalyst used for the synthesis of fishbone CNFs. Fig. 7(c)–(e) presents the element mapping of carbon, nickel and molybdenum. As expected, the mapping of carbon essentially mimics the picture of the CNFs. The X-ray intensity of Ni and Mo, and in particular Mo, is mostly

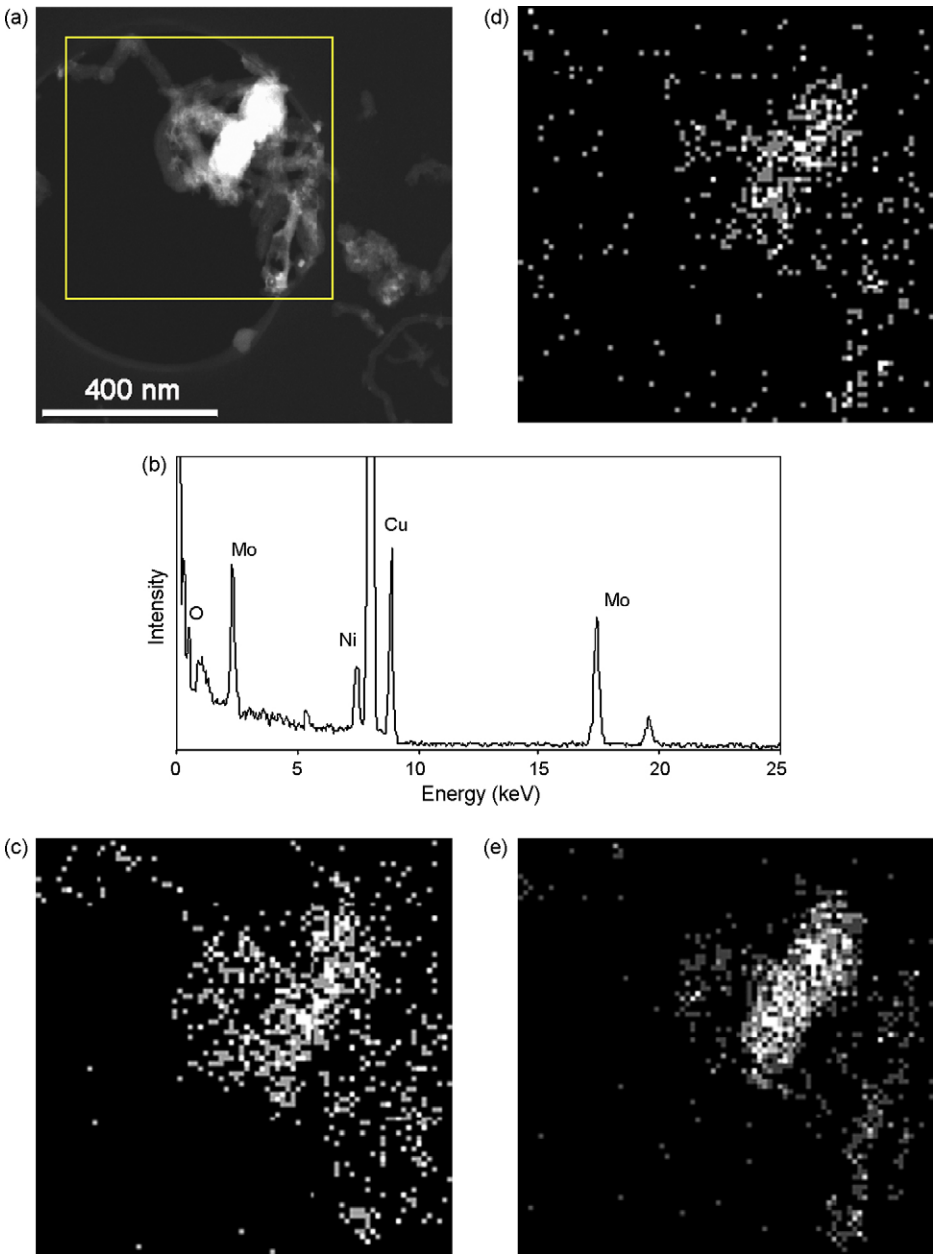

Fig. 7. STEM-EDX characterization of the NiMo/Fishbone catalysts; (a) an overview of the mapping area, (b) sum spectrum of different components, (c) carbon mapping, (d) nickel mapping, and (e) molybdenum mapping.

concentrated in the bright area observed in Fig. 7(a). This means that some of the NiMo and/or Mo oxides conglomerate in this area. NiMo and/or Mo oxides particles also deposit on the lower right part of the CNF surfaces, as shown in Fig. 7(e). However, the X-ray signal of molybdenum does not come from the whole CNF surfaces, which seems to be in consistence with XRD results that the oxides are deposited as separate particles instead of a layer.

The reason to select the CNFs with fishbone and platelet structures in this study is that they have more edge sites exposed on the surfaces compared with CNTs, which have more inert basal planes. Previous studies have shown that the CNFs are superior to CNTs as catalyst supports in reactions such as hydrogenation of crotonaldehyde [14] and oxidative dehydrogenation of ethylbenzene [15]. The edge sites are the anchoring sites for catalyst precursors. Indeed, the edge sites of the CNFs have been successful in providing anchoring sites for the deposition of small crystalline molybdenum oxides particles, as observed in the TEM images (Fig. 6(a)–(c)). Nevertheless, the edge sites are probably not favored for the deposition of a molybdenum layer, which is a precondition for very active molybdenum HDS catalysts. In this regard, CNTs with more perfect surfaces could be more suitable as support, because CNTs have often been used as templates for the preparation of metal oxide or sulfide layers on CNTs [32]. Of course, it could also be that the standard incipient wetness method used in this study is not optimal for the preparation of monolayer molybdenum on the CNFs.

3.4. Hydrodesulfurization of thiophene

Fig. 8 presents the thiophene conversion as a function of time on the supported Mo catalysts. The thiophene conversion is relatively low at 4–5% for both catalysts. The catalyst activity decreases

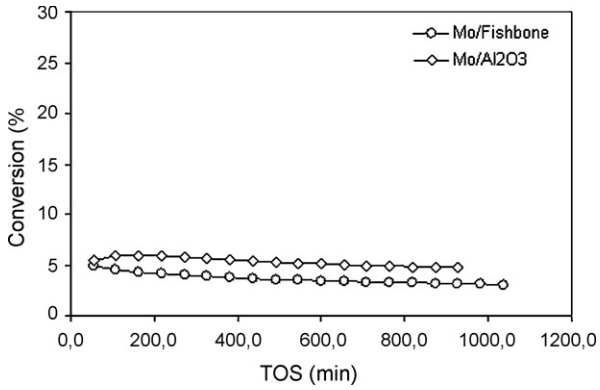

Fig. 8. The conversion of thiophene during time on stream on the supported Mo catalysts.

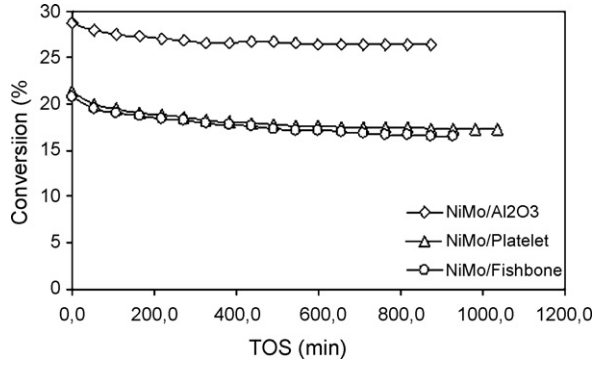

Fig. 9. The conversion of thiophene during time on stream on the supported NiMo catalysts.

during time on stream but the deactivation rate is relatively low. After around 400–600 min the conversion curves level out, indicating a stabilization of the catalysts after initial deactivation [18]. The thiophene conversions on different catalysts after the system being stabilized for 381 min are summarized in Table 1.

Fig. 9 shows the thiophene conversion during time on stream on the supported NiMo catalysts. Again, the thiophene conversion decreases over time, albeit at a very low rate, and after around 400–600 min the conversion curves level out. The $NiMo/Al_2O_3$ catalyst obtains the highest thiophene conversion of 26.5%, higher than the conversion obtained on the CNFs supported catalysts, which have conversions around 18%. The NiMo/Platelet catalyst has a slightly higher activity than that of NiMo/Fishbone, but the difference is small.

For the CoMo series, the $CoMo/Al_2O_3$ catalyst again has the highest activity, with a thiophene conversion of 14.6% (Fig. 10), about half the activity of the $NiMo/Al_2O_3$ catalyst. The CoMo/Fishbone and CoMo/Platelet catalysts show conversions of 12.7% and 11.9%, respectively.

The correlation between the dispersion of the MoO_x phase in the calcined catalysts, the dispersion of the MoS_2 phase under reaction conditions, and the HDS activity of different catalysts have been demonstrated previously [23]. The catalysts supported on γ-Al_2O_3 have the highest activity amongst the prepared catalysts with the same metal loading, apparently due to their highly dispersed nature, as proved by the absence of any crystalline oxide phases in the XRD study. Iwata et al. [33] proposed a strong effect of the crystal structure on the HDS activity of the catalysts: the poorly crystallized structure provided a larger number of catalytically active sites than the well-crystallized structure. The formation of crystalline MoO_3 phases on the CNFs will result in lower HDS activity compared with the alumina supported catalysts.

On the other hand, it has also been shown that there is a good correspondence of the reducibility of the molybdenum catalysts and their HDS activity [27]. It is well known that the active phase of HDS catalysts is MoS_2, in which Mo is in the Mo^{4+} state and the oxide needs to be transformed into sulfide before being active [34]. A high reducibility will contribute to an increased number of sulfided species for the working catalysts. This can explain the higher activity of the CoMo/Fishbone than the CoMo/Platelet catalyst, because CoMo/Fishbone is easier to reduce than CoMo/Platelet, as shown in Fig. 4. However, the alumina supported catalysts are much more difficult to reduce than the CNFs supported catalysts. Therefore, there is a trade-off between the dispersion and reducibility, and the catalyst structure and dispersion could be more important than the ease of reduction and sulfidation for the HDS activity.

The CoMo/Platelet catalyst calcined at 500 °C is slightly more active (13.2% conversion) than the catalyst calcined at 350 °C (11.9% conversion), as shown in Fig. 11. This can be explained by the presence of MoO_2 phase instead of MoO_3 after the calcination at 500 °C, because the sulfidation of MoO_2 is easier than the corresponding reduction and sulfidation of MoO_3.

Ni and Co are well-known promoters for Mo based HDS catalysts [2,17,21]. Compared with the molybdenum-only catalysts, the CoMo or NiMo catalysts show 3–6 times higher activity. The NiMo catalysts are more active than the CoMo series, hence nickel seems to be a better promoter compared with cobalt for thiophene HDS in this study. Nevertheless, the higher activity can be explained by the reducibility of the NiMo catalysts, because all of the NiMo catalysts are reduced at a lower temperature than the corresponding CoMo catalysts, as demonstrated by TPR study.

Interestingly, the Co/CNFs have a high activity for thiophene HDS, as shown in Fig. 12. The Co/Platelet and Co/Fishbone catalysts

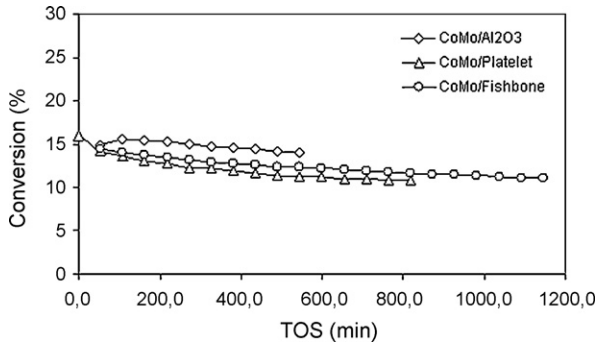

Fig. 10. The conversion of thiophene during time on stream on the supported CoMo catalysts.

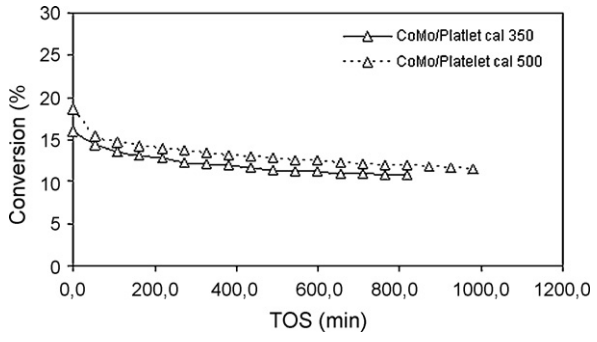

Fig. 11. The conversion of thiophene during time on stream on the CoMo/Platelet catalysts calcined at different temperatures.

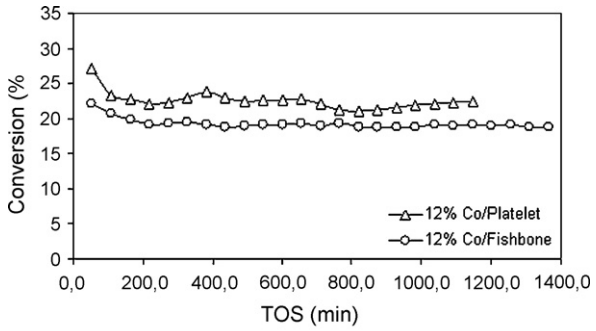

Fig. 12. The conversion of thiophene during time on stream on the supported Co catalysts.

have stable thiophene conversion of 23.0% and 19.2%, respectively. This pronounced activity is even higher than the NiMo/CNFs catalysts (Fig. 9). This is contradictory because in HDS catalysis Co has normally been considered as the promoter of the Mo activity. However, it has been shown by other studies that cobalt and nickel sulfides, when supported on carbon, have substantial intrinsic activities for thiopene HDS compared to molybdenum or tungsten sulfides [35–37]. Based on these experimental observations, it has been suggested that Co is the active species and Mo is a structural promoter of the CoMo systems. Hence the role of Co and Ni sulfides, at least when supported on carbon materials, may not be limited to promoting MoS_2 or WS_2. The activities of alumina and silica supported cobalt-only HDS catalysts have also been reported recently [38]. The high thiophene HDS activity of CNFs supported cobalt catalysts is of potential promise and worth further study. There might be an optimal Co/Mo ratio and loading, probably different from those for conventional alumina supports, which will make the CNFs supported CoMo catalysts with high activity.

4. Conclusions

XRD results have shown that the molybdenum oxides appear to be dispersed as monolayer on the alumina support, but as small crystalline particles on the CNFs supports, which is confirmed by TEM characterization. Ni and Co promotion leads to better dispersion of the molybdenum oxides, as demonstrated by the smaller diffraction peaks in the XRD study. There are no obvious differences between fishbone and platelet CNFs in terms of the resulting catalyst phases.

TPR analysis shows that the alumina supported catalysts are much more difficult to reduce than the corresponding CNFs supported catalysts, due to the strong interaction between the alumina support and the metal particles. The NiMo catalysts are always easier to reduce than the CoMo catalysts.

Thiophene HDS reaction confirmed that the promotion by Ni or Co resulted in a significant increase of the catalytic activity. The NiMo catalysts are more active than the CoMo catalysts, which can be explained by their ease of reduction thus sulfidation. Although much more difficult to reduce, the alumina supported catalysts exhibited higher activity than the corresponding CNFs supported catalysts, due to their much higher dispersion. Therefore, a high activity is associated with high dispersion and reducibility, and the dispersion seems to be more important for the high activity in thiophene HDS. The CNFs supported cobalt-only catalysts have shown surprisingly high activity, which deserves further study.

The edge sites of the fishbone and platelet CNFs might not be favored for the molybdenum oxides to form a monolayer on their surfaces. Either the preparation method should be improved or other carbon nanostructures such as CNTs could be used to increase their activity for potential practical applications.

Acknowledgements

The financial support from StatoilHydro Research Center is greatly acknowledged. The authors also thank Heimir Magnusson for help with the TEM experiments.

References

[1] M. Breysse, P. Afanasiev, C. Geantet, M. Vrinat, Catal. Today 86 (2003) 5–16.
[2] Y. Okamoto, T. Kubota, Catal. Today 86 (2003) 31–43.
[3] B. Scheffer, P. Arnoldy, J.A. Moulijn, J. Catal. 112 (1988) 516–527.
[4] J.J. Lee, S. Han, H. Kim, J.H. Koh, T. Hyeon, S.H. Moon, Catal. Today 86 (2003) 141–149.
[5] Z. Vit, Fuel 72 (1993) 105–107.
[6] H. Farag, D.D. Whitehurst, K. Sakanishi, I. Mochida, Catal. Today 50 (1999) 9–17.
[7] H. Farag, I. Mochida, K. Sakanishi, Appl. Catal. A 194–195 (2000) 147–157.
[8] P. Serp, M. Corrias, P. Kalck, Appl. Catal. A 253 (2003) 337–358.
[9] K.P. de Jong, J.W. Geus, Catal. Rev. Sci. Eng. 42 (2000) 481–510.
[10] M.K. van der Lee, A.J. van Dillen, J.H. Bitter, K.P. de Jong, J. Am. Chem. Soc. 127 (2005) 13573–13582.
[11] K. Dong, X. Ma, H. Zhang, G. Lin, J. Nat. Gas Chem. 15 (2006) 28–37.
[12] H. Chen, X. Zhou, H. Shang, C. Liu, J. Qiu, F. Wei, J. Nat. Gas Chem. 13 (2004) 209–217.
[13] H. Shang, C. Liu, R. Zhao, M. Wu, F. Wei, Chinese J. Chem. 22 (2004) 1250–1256.
[14] F. Salman, C. Park, R.T.K. Baker, Catal. Today 53 (1999) 385–394.
[15] T. Zhao, W. Sun, X. Gu, M. Rønning, D. Chen, Y. Dai, W. Yuan, A. Holmen, Appl. Catal. A 323 (2007) 135–146.
[16] Z. Yu, Ø. Borg, D. Chen, B.C. Enger, V. Frøseth, E. Rytter, H. Wigum, A. Holmen, Catal. Lett. 109 (2006) 43–47.
[17] M. Egorova, R. Prins, J. Catal. 241 (2006) 162–172.
[18] P. Steiner, Kinetic and deactivation studies of hydrodesulfurization catalysts, Ph.D. Thesis, NTNU, Trondheim, Norway, 2002.
[19] Z. Yu, D. Chen, B. Tøtdal, A. Holmen, J. Phys. Chem. B 109 (2005) 6096–6102.
[20] M.L. Toebes, J.H. Bitter, A.J. van Dillen, K.P. de Jong, Catal. Today 76 (2002) 33–42.
[21] G.M.K. Abotsi, A.W. Scaroni, Fuel Process. Technol. 22 (1989) 107–133.
[22] G.L. Bezemer, A. van Laak, A.J. van Dillen, K.P. de Jong, Stud. Surf. Sci. Catal. 147 (2004) 259.
[23] J.A. Berhwerff, M. Jansen, B.G. Leliveld, T. Visser, K.P. de Jong, B.M. Weckhuysen, J. Catal. 243 (2006) 292–302.
[24] J. Matos, J.L. Brito, J. Laine, Appl. Catal. A 152 (1997) 27–42.
[25] M. Kouzu, Y. Kuriki, F. Hamdy, K. Sakanishi, Y. Sugimoto, I. Saito, Appl. Catal. A 265 (2004) 61–67.
[26] H. Shang, Y. Xu, H. Zhao, C. Liu, Acta Petrolei Sin. 20 (2004) 81–89.
[27] H. Shang, Y. Xu, H. Zhao, C. Liu, J. Mol. Catal. (China) 18 (2004) 41–46.
[28] G. Jacobs, T.K. Das, Y. Zhang, J. Li, G. Racoillet, B.H. Davis, Appl. Catal. A 233 (2002) 261–281.
[29] Ø. Borg, S. Eri, E.A. Blekkan, S. Storsæter, H. Wigum, E. Rytter, A. Holmen, J. Catal. 248 (2007) 89–100.
[30] M.A. Al-Saleh, M.M. Hossain, M.A. Shalabi, T. Kimura, T. Inui, Appl. Catal. A 253 (2003) 453–459.
[31] D. Li, I. Atake, T. Shishido, Y. Oumi, T. Sano, K. Takehira, J. Catal. 250 (2007) 299–312.
[32] B.C. Satishkumar, A. Govindaraj, M. Nath, C.N.R. Rao, J. Mater. Chem. 10 (2000) 2115–2119.
[33] Y. Iwata, K. Sato, T. Yoneda, Y. Miki, Y. Sugimoto, A. Nishijima, H. Shimada, Catal. Today 45 (1998) 353–359.
[34] J. Grimblot, Catal. Today 41 (1998) 111–128.
[35] J.C. Duchet, E.M. van Oers, V.H.J. de Beer, R. Prins, Appl. Catal. 30 (1987) 21–31.
[36] V.H.J. de Beer, J.C. Duchet, R. Prins, J. Catal. 72 (1981) 369–372.
[37] J.P.R. Vissers, V.H.J. de Beer, R. Prins, J. Chem. Soc., Faraday Trans. 1 (83) (1987) 2145–2155.
[38] A.M. Venezia, R. Murania, G. Pantaleo, G. Deganello, J. Mol. Catal. A 271 (2007) 238–245.